The International Journal of Advanced Manufacturing Technology (2018) 95:4141–4152
https://doi.org/10.1007/s00170-017-1556-7

ORIGINAL ARTICLE

Modeling and simulation of milling forces in milling plain woven carbon fiber-reinforced plastics

Fei Su [1,2] · Juntang Yuan [3] · Fujian Sun [1,2] · Zhenhua Wang [3] · Zhaohui Deng [1,2]

Received: 23 September 2017 / Accepted: 26 December 2017 / Published online: 5 January 2018

Abstract
Woven CFRP composites are increasingly applied in different industrial sectors. Excessive milling forces can involve some undesirable consequences such as rapid tool wear, surface burning, burrs, delamination, etc., during the milling of CFRP. Reasonably predicting force is of great significance to improve the machining quality and the tool life. A methodology is developed for predicting the milling forces by transforming specific cutting energies derived from the theoretical model of orthogonal cutting. In this methodology, the structural features of the plain-woven structure are carefully observed and analyzed. It is shown that all the average force coefficients regularly change with the rotation angle. The theoretical results applying these average force coefficients agree well with the measuring data. Furthermore, the maximal average of the cutting forces can be successfully predicted. All the average absolute values of relative errors between predictive and measured values of the cutting forces max-means are less than 10%. It is shown that the method applying the average force coefficients is capable of predicting the cutting forces in milling of plain-woven CFRP and over the entire range of rotation angles from 0 to 180°. The results can provide a reference for the prediction and the control of cutting forces in actual milling of plain-woven carbon fiber-reinforced plastics.

Keywords Plain-woven carbon fiber-reinforced plastic (PW CFRP) · Milling forces · Theoretical model · Specific cutting energies

1 Introduction

Carbon fiber-reinforced polymer (CFRP) composites have been widely applied in many industries, such as aerospace, construction, transportation, etc., due to the favorable characteristics, for example, lightweight, high strength, and high modulus [1–5]. Usually, it is necessary to carry out a post-machining operation to meet the required geometry tolerances and surface quality of all the near net-shape CFRP parts. Generally, the milling process is considered as one of the most common finishing operations. It is well known that some different kinds of machining problems may be vulnerable to generate, such as fiber pull-out, burrs, delamination, intensive tool wear, and so on, due to the heterogeneity and anisotropic behavior of the CFRP materials [6, 7].

Milling force is an important intermediate variable related to machining defects and tool wear [8–10]. Hence, reasonably predicting force is of great significance to further understand the milling process of CFRP, and is an important guide to the rational choice of the cutting parameters to reduce the defects and decrease the tool wear. So far, the modeling method of the milling forces can be divided into two kinds, i.e., the empirical method based on experiment data and the analytical method according to the mechanistic [11–14]. The former is not based on physics of the process and needs to redetermine the correlation coefficients when the tool geometry or materials change. The prediction accuracy of the latter depends, to a great extent, on the specific energies or specific force coefficients [14].

There have been numerous attempts to create mathematical models to predict the milling forces using the analytical method,

"This is an original paper which has neither previously, nor simultaneously, in whole or in part been submitted anywhere else."

✉ Fei Su
sfeihe@163.com

[1] Hunan Provincial Key Laboratory of High Efficiency and Precision Machining of Difficult-to-Cut Material, Hunan University of Science and Technology, Xiangtan 411201, China

[2] Intelligent Manufacturing Institute of HNUST, Hunan University of Science and Technology, Xiangtan 411201, China

[3] School of Mechanical Engineering, Nanjing University of Science and Technology, Nanjing 210094, China

during the metals cutting. But unlike metals, the cutting mechanism of the composite materials is brittle fracture instead of plastic deformation, and is greatly affected by the fiber direction. Extensive published studies have indicated that the specific energies of the CFRP depend on the fiber orientation, due to the anisotropic and inhomogeneous material properties. Sheikh-Ahmad et al. [15] described the specific energies as a function of fiber orientation by the multiple regression analysis (MR) and committee neural network approximation (CN). Then, a cutting model was developed based on these energies and the cutting geometry. It was found that the predictive model based on neural network performed better than on regression analysis. Kalla et al. [8] proposed a methodology combining the mechanistic modeling techniques and artificial neural network (ANN) approximation to obtain a predictive milling force for helical end milling of CFRP. The specific energies in tangential and radial directions were calculated with ANN data which was obtained from a series of UD-CFRP orthogonal up-milling experiments. It was found that the model predictions were in good agreement with the experimental data in milling UD-CFRP, but with lesser agreement in multidirectional laminate. Karpat et al. [16] presented a mechanistic cutting force model for milling CFRP based on the cutting force coefficients which were calculated as a function of fiber cutting angle. Han et al. [17] conducted a series of experiments with multitooth cutter and calculated the milling force coefficients of unidirectional CFRP for typical directions (45°, 0°, -45°, 90°) with different feed speeds. And the milling forces were modeled and simulated using an instantaneous rigid force model. They obtained good results for multidirectional laminates. Above these models all attempt to determine the specific force coefficients during the milling forces modeling. However, there are still some problems yet to be overcome. For example, it may need a great deal of experiments to obtain the specific force coefficients for different tool-workpiece combinations, and this modeling process may be rather complicated. What is more, the existing functional relationships between the specific force coefficients and the fiber orientation almost target for unidirectional laminates, but seldom for plain-woven laminates.

In general, the specific cutting energies may be acquired from the mechanistic modeling of the orthogonal cutting [18]. Then, using these specific energies, the cutting forces may be predicted in terms of a number of relevant parameters, such as the chip dimensions, tool geometries, and process conditions. By now, numerical mechanism modeling which can reveal the physical essence of the material failure and removal to a certain extent have been tried out for the orthogonal cutting. Takeyama et al. [19] presented a cutting force model in orthogonal cutting of the unidirectional laminates with the fiber directions in the range from 0 to 90°. But it is difficult to compute the shear plane angle due to the powder chips. Still, Bhatnagar et al. [20] noted that a crack propagation plane existed along the fiber direction and used the fiber angle instead of the shear plane angle. Zhang et al. [21] proposed that the chipping was the result of zigzag cracking of the fibers and the debonding of the fiber-matrix interface. The shear plane angle was treated as a function of the rake angle. Jahromi et al. [22] presented the cutting forces via the classical beam theory and regarded the fiber as a cantilever beam. In their model, the length of chip and the number of the fibers in the chip were determined to calculate the total cutting forces. After that, Qi et al. [23] developed this model considering the supporting effect during the cutting of a single fiber. But the fiber orientation was in the range from 0 to 90°. For continuing the Qi et al. research, Chen et al. [24] also applied the elastic foundation beam theory and the minimum potential energy principle (MPEP) to establish the mechanical model for the entire range of fiber directions. Xu et al. [25, 26] and Niu et al. [27] presented the micro-mechanical model during the orthogonal cutting of a single fiber, also via the elastic foundation beam theory. However, in order to calculate the cutting forces, most of these models need a number of relevant parameters of the microstructure, and the computing processes are time consuming and extremely complicated. In Zhang's model, there were three distinctive cutting regions, which can reveal the physical essence of the material failure and removal to a certain extent. And this model may be a simple and reliable solution for the orthogonal cutting forces. Besides this, this model had been successfully used for the prediction of the thrust force and torque generated in the drilling of CFRP [28]. Thus, compared with the other models, this model is suitable for practical applications in the milling force modeling.

Woven CFRP composites are increasingly applied in different industrial sectors due to their some advantages comparing with the unidirectional laminates [29]. However, according to the analyses above, few previous reports on the plain-woven CFRP specific force coefficients acquired from the mechanistic modeling of the orthogonal cutting. Especially, the research that considers the woven structure in the specific cutting energies solving process is even rarer. In this paper, the plain-woven CFRP specific force coefficients will be derived based on the Zhang's orthogonal cutting model, according to the structural features of the plain-woven structure. Then, the milling forces of the plain-woven CFRP will be predicted by using these specific energies. This research can provide a theoretical basis for cutting parameter optimization and tool geometry optimization in the future research.

2 Mechanistic force modeling

2.1 Milling force modeling

In general, the milling process is the periodical interrupted cutting using the multi-edges end mill, and the cutting depth per tooth presents periodic variation with the tool rotation angle. A helical end mill with a helix angle δ, number of flutes

N, tool radius R, and the axial depth of cut a_p are assumed. Each flute is divided into K small segments along the tool axis. Then, the infinite cutting forces (tangential, radial, and axial) acting on the individual segments can be similarly considered as the corresponding cutting forces in orthogonal cutting with the helix angle $\delta = 0$, as shown in Fig. 1. The directions of forces X, Y, and Z are along the feed, normal, and axial directions, respectively.

By this stage, the infinite cutting forces acting on the oblique cutting edge of flute j can be determined by the cutting area and the tool-workpiece contact length, and it is expressed as [30, 31]:

$$\begin{Bmatrix} \mathrm{d}F_{r,j}(t,z) \\ \mathrm{d}F_{t,j}(t,z) \\ \mathrm{d}F_{a,j}(t,z) \end{Bmatrix} = g(\phi_j)\left[\begin{Bmatrix} K_{\mathrm{re}} \\ K_{\mathrm{te}} \\ K_{\mathrm{ae}} \end{Bmatrix}\cdot dz + \begin{Bmatrix} K_{\mathrm{rc}} \\ K_{\mathrm{tc}} \\ K_{\mathrm{ac}} \end{Bmatrix}\cdot h_{d,j}(t,z)\cdot dz\right] \quad (1)$$

where, dz is the thickness of each disk and K_{tc}, K_{rc}, and K_{ac} are the cutting force coefficients in tangential, radial, and axial directions, respectively. K_{te}, K_{re}, and K_{ae} are the corresponding edge force coefficients; $g(\varphi_j)$ is used to define whether the tooth j is in cut or not, as the tooth is cutting $g(\varphi_j) = 1$, instead, $g(\varphi_j) = 0$, as shown in Eq. (2). $h_{d,j}(t,z)$ is the chip thickness of tooth j, as shown in Eq. (3):

$$g(\phi_j) = \begin{cases} 1 & \phi_{st} \le \phi_j \le \phi_{ex} \quad \text{cutting} \\ 0 & \phi_j < \phi_{st} \text{或} \phi_j > \phi_{ex} \quad \text{don't cut} \end{cases} \quad (2)$$

$$h_{d,j}(t,z) = f_z \cdot \sin\phi_{jl} \quad (3)$$

where, f_z is the tangential feed rate per tooth, φ_{jl} is the l-th segment immersion angle of the j-th cutting edge, and φ_{st} and φ_{ex} are the entrance angle and the exit angle, respectively [32].

It is assumed that the flutes are uniformly distributed on the end mill. Then, the immersion angle φ_{jl} can be written as [14]:

$$\phi_{jl} = \phi_{10} + (j-1)\cdot\phi_p + \frac{ldz\tan\delta}{R} \quad (4)$$

where φ_p is the pitch angle and $\varphi_p = 2\pi/N$, N is the total flutes number of the cutter, and φ_{10} is the first rotation angle of reference cutting edge.

Therefore, the sum of the tangential, radial, and axial cutting forces on each tooth segment is the total forces acting on the cutter in corresponding directions, and can be given by [14]:

$$\begin{Bmatrix} F_{r,j}(t) \\ F_{t,j}(t) \\ F_{a,j}(t) \end{Bmatrix} = \begin{Bmatrix} K_{\mathrm{re}} \\ K_{\mathrm{te}} \\ K_{\mathrm{ae}} \end{Bmatrix}\cdot a_p + \begin{Bmatrix} K_{\mathrm{rc}} \\ K_{\mathrm{tc}} \\ K_{\mathrm{ac}} \end{Bmatrix}\cdot h_{d,j}(t)\cdot a_p \quad (5)$$

Three-direction elemental cutting forces from Eq. (5) can be resolved into X, Y, and Z directions by the following transformation [14, 33]:

$$\begin{Bmatrix} F_x(t) \\ F_y(t) \\ F_z(t) \end{Bmatrix} = \begin{bmatrix} -\sin\phi_j(t) & -\cos\phi_j(t) & 0 \\ \cos\phi_j(t) & -\sin\phi_j(t) & 0 \\ 0 & 0 & 1 \end{bmatrix}\begin{Bmatrix} F_r(t) \\ F_t(t) \\ F_a(t) \end{Bmatrix} = \begin{bmatrix} -\sin\phi_j(t) & -\cos\phi_j(t) & 0 \\ \cos\phi_j(t) & -\sin\phi_j(t) & 0 \\ 0 & 0 & 1 \end{bmatrix}\cdot\sum_{j=1}^{N}\begin{Bmatrix} F_{r,j}(t) \\ F_{t,j}(t) \\ F_{a,j}(t) \end{Bmatrix} \quad (6)$$

In general, the cutting force coefficients of CFRP are highly dependent on the fiber orientation. These cutting force coefficients can be obtained in the cutting experiments, but the process is quite cumbersome and the results have certain limitations. In addition, comparing with the cutting forces F_x and F_y, the axial cutting force F_z is quite small, and it has a little influence on the cutting process. Here, the cutting force models in X and Y directions are only analyzed.

2.2 Cutting force coefficients of CFRP

The plain-woven CFRP is made from the woven sheets of carbon fibers which are weaved by the warp yarns and the fill yarns. The plain-woven CFRP and the fabric structure are shown in Fig. 2. However, the warp yarns and the fill yarns cannot be able to distinguish after the forming of CFRP with a plain weave fabric. For easy distinguishing, the fiber whose axis is parallel to the feed direction is regarded as the fill fiber. The fiber whose axis is perpendicular to the feed direction is treated as the warp fiber. It can be seen that there is $\pi/2$ difference between the fiber orientation of the warp fiber and that of the fill fiber with the same rotation angle, as given by:

$$\begin{cases} \theta_1 = \phi \\ \theta_2 = \dfrac{\pi}{2} + \phi \end{cases} \quad (7)$$

where φ is the rotation angle of the cutter and θ_1 and θ_2 are the fiber direction of the fill fiber and the warp fiber, respectively.

(1) Cutting force coefficients of unidirectional CFRP

As the helix angle $\delta = 0°$, the cutting process of the individual segments can be regarded as an independent orthogonal cutting process. In order to simplify the

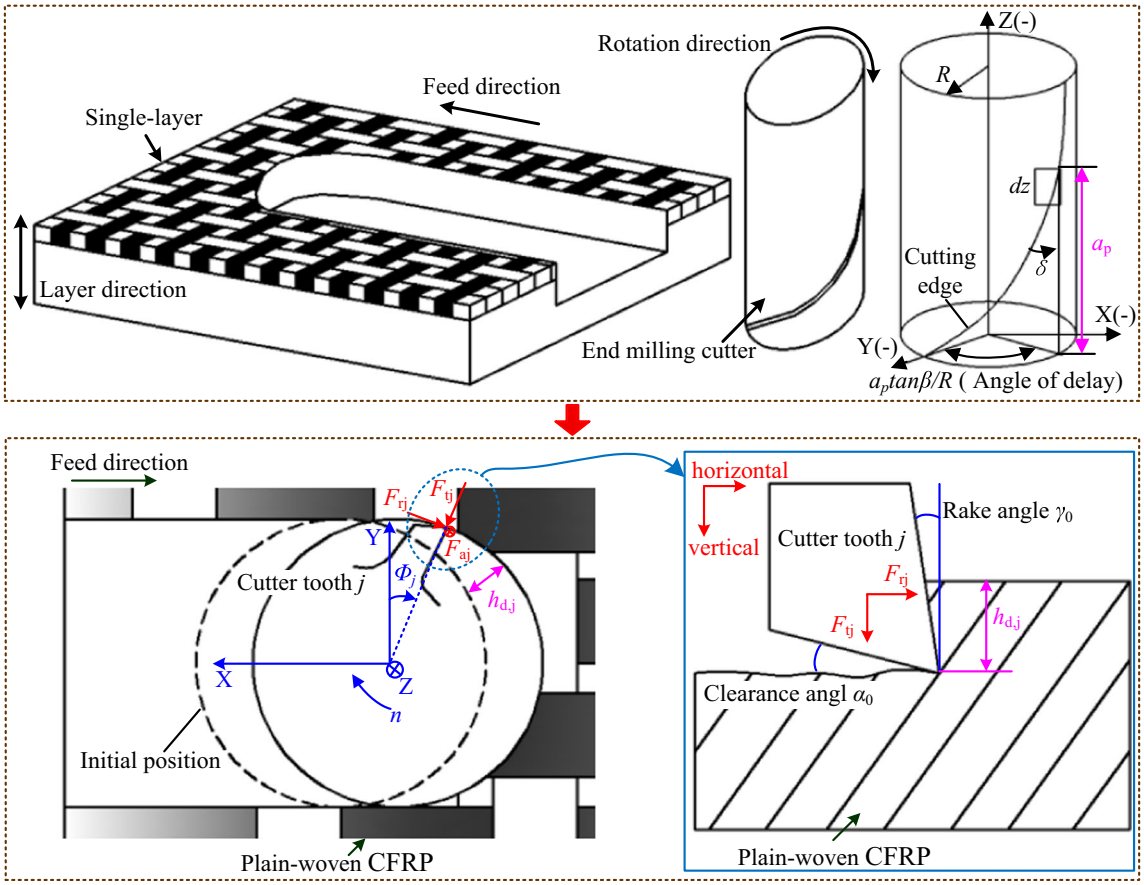

Fig. 1 Milling force model of helical cut edges

modeling process, the fiber orientation θ is assumed to be less than 90°, and the proposed model is also valid for the fiber orientation $\theta > 90°$ [28]. The orthogonal cutting model is demonstrated in Fig. 3. It is suggested that there are three key deformation regions in the cutting zone of a UD-CFRP laminate. During cutting, the fiber fracture and the matrix shear failure are the main mechanisms of the material removal. Knowledge from research studies and practical experience indicates that the fibers are a key material in CFRP for the generation of the cutting forces, but the resin matrix has minimal effect on the generation of the cutting forces [14]. Hence, it is supposed to ignore the effect of the resin matrix. During the further feed motion of the cutter, the fiber fractures when the internal stress exceeds its shear strength, then the fiber slip along the fiber-matrix interfaces. And when the internal stress

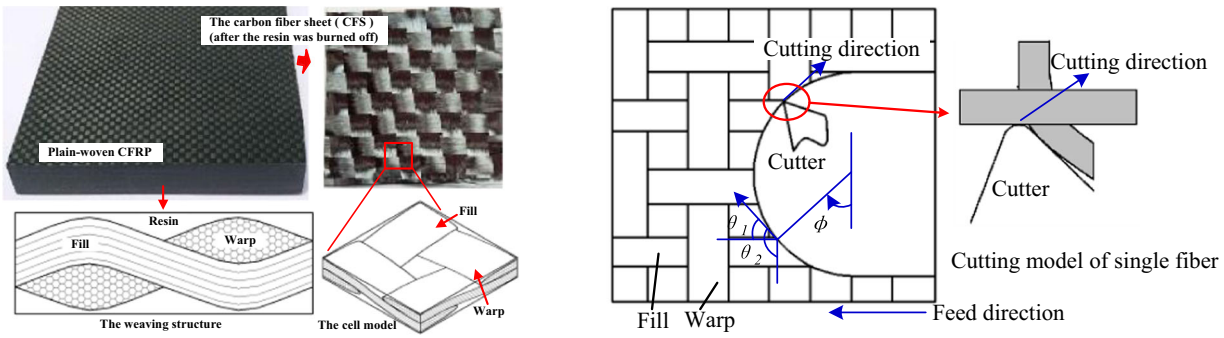

(a) Plain-woven CFRP and the weaving structure (b) Cutting model of the carbon fiber sheet (CFS)

Fig. 2 Plain-woven CFRP and its cutting model. **a** Plain-woven CFRP and the weaving structure. **b** Cutting model of the carbon fiber sheet (CFS)

exceeds the interfacial shear strength, the chip is formed [21].The chipping along an overall shear plane is the result of a zigzag cracking of the fibers perpendicular to the fiber axes and the fiber-matrix interface debonding parallel to the fiber axes [21], as shown in Fig. 3. The first region results in a chip formation in front of the rake face, and is called as chipping region or region A. The second region is under the nose of the cutter and called as pressing region or region B. The third region is at the back of the cutter nose and called as bouncing region or region C. All the regions are denoted in Fig. 3.

It is assumed that the total cutting force can be calculated by adding up the forces in all the three regions. The horizontal and vertical cutting forces in each region can be obtained as follows [21]:

(a) In chipping region or region A:

$$\begin{cases} F_{c1} = \dfrac{a_c\tau_1 b[\sin\varphi\tan(\varphi+\beta-r_0)+\cos\varphi]}{\frac{\tau_1}{\tau_2}\cos(\theta-\varphi)\sin\theta-\sin(\theta-\varphi)\cos\theta} \\ F_{t1} = \dfrac{a_c\tau_1 b[\cos\varphi\tan(\varphi+\beta-r_0)-\sin\varphi]}{\frac{\tau_1}{\tau_2}\cos(\theta-\varphi)\sin\theta-\sin(\theta-\varphi)\cos\theta} \end{cases} \tag{8}$$

(b) In pressing region or region B:

$$\begin{cases} F_{c2} = \dfrac{\pi r_e E_3 b}{8(1-\nu^2)}(\sin\theta+\mu\cos\theta) \\ F_{t2} = \dfrac{\pi r_e E_3 b}{8(1-\nu^2)}(\cos\theta-\mu\sin\theta) \end{cases} \tag{9}$$

(c) In bouncing region or region C:

$$\begin{cases} F_{c3} = \dfrac{r_e E_3 b\mu}{2(1-\nu^2)}(\cos\alpha_0)^2 \\ F_{t3} = \dfrac{r_e E_3 b\mu}{2(1-\nu^2)}(1-\mu\cos\alpha_0\sin\alpha_0) \end{cases} \tag{10}$$

The total forces are the summation of the corresponding components from the above three regions, and can be written as:

$$\begin{cases} F_{cz} = F_{c1}+F_{c2}+F_{c3} \\ F_{tz} = F_{t1}+F_{t2}+F_{t3} \end{cases} \tag{11}$$

Namely:

$$\begin{cases} F_{cz} = \dfrac{\tau_1[\sin\varphi\tan(\varphi+\beta-r_0)+\cos\varphi]}{\frac{\tau_1}{\tau_2}\cos(\theta-\varphi)\sin\theta-\sin(\theta-\varphi)\cos\theta}a_c b+\left[\dfrac{\pi r_e E_3}{8(1-\nu^2)}(\sin\theta+\mu\cos\theta)+\dfrac{r_e E_3\mu}{2(1-\nu^2)}(\cos\alpha_0)^2\right]b \\ F_{tz} = \dfrac{\tau_1[\cos\varphi\tan(\varphi+\beta-r_0)-\sin\varphi]}{\frac{\tau_1}{\tau_2}\cos(\theta-\varphi)\sin\theta-\sin(\theta-\varphi)\cos\theta}a_c b+\left[\dfrac{\pi r_e E_3}{8(1-\nu^2)}(\cos\theta-\mu\sin\theta)+\dfrac{r_e E_3\mu}{2(1-\nu^2)}(1-\mu\cos\alpha_0\sin\alpha_0)\right]b \end{cases} \tag{12}$$

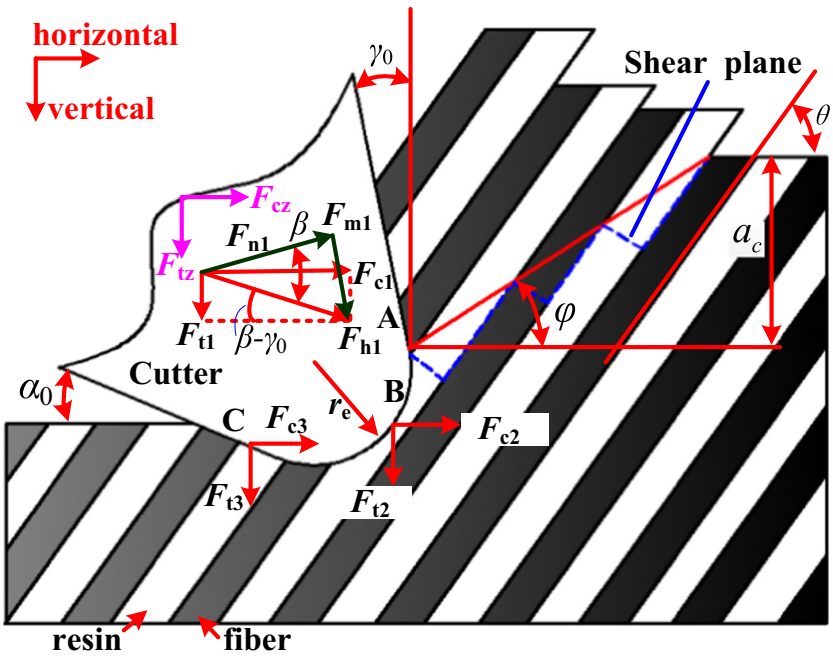

Fig. 3 Cutting model of the unidirection CFRP

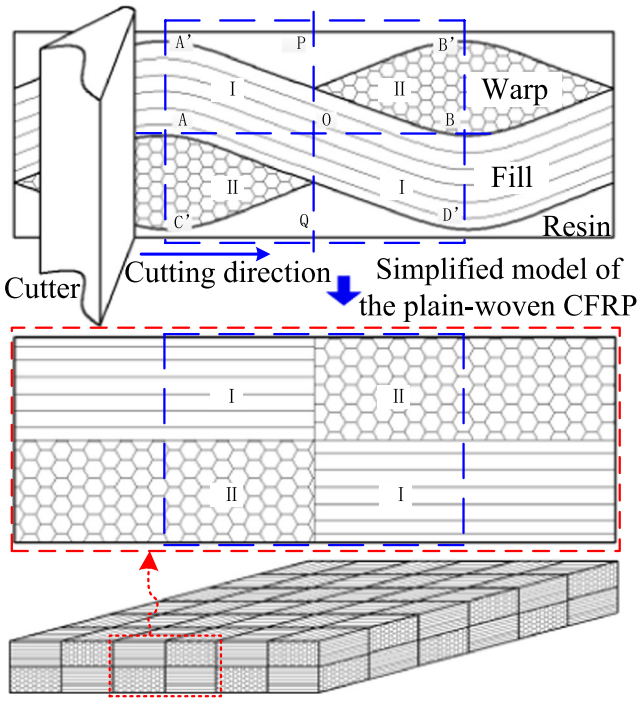

Fig. 4 Simplified model of the plain-woven CFRP

where F_{c1}, F_{c2}, and F_{c3} are the horizontal cutting forces in regions A, B, and C, respectively. F_{t1}, F_{t2}, and F_{t3} are the vertical cutting forces in regions A, B, and C, respectively. F_{m1}, F_{n1}, and F_{h1} are the cutter-chip friction force, the normal force, and the total force in region A, respectively. a_c is the real cut depth; φ is the shear plane angle and can be calculated by $\varphi = atan\left(\frac{\cos\gamma_0}{1-\sin\gamma_0}\right)$ [21]; β is the friction angle between a chip and the rake face of the cutting lip; γ_0 is the rake angle; α_0 is the clearance angle; b is the contact width; τ_1 and τ_2 are the shear strength of the fiber and that of the matrix, respectively; r_e is the nose radius; E_3 is the effective elastic modulus of the CFRP in third orientation (perpendicular to the laminates); μ is the friction coefficient; ν is the Poisson's ratio; and F_{cz} and F_{tz} are the total horizontal and vertical cutting forces, respectively.

Obviously, for the cutting processes of the individual segments, h_{dj} and a_p are the cutting thickness and the cutting width, respectively. So $h_{dj} = a_c$, $a_p = b$. Additionally, in essence, $F_{r,j} = F_{tz}$, $F_{t,j} = F_{cz}$. Then, comparing with Eq. (5) and Fig. 1, the cutting force coefficients and the corresponding edge force coefficients can be derived as:

$$\begin{cases} K_{rc} = \dfrac{\tau_1[\sin\varphi\tan(\varphi+\beta-r_0)+\cos\varphi]}{\frac{\tau_1}{\tau_2}\cos(\theta-\varphi)\sin\theta-\sin(\theta-\varphi)\cos\theta} \\ K_{re} = \dfrac{\pi r_e E_3}{8(1-\nu^2)}(\sin\theta+\mu\cos\theta)+\dfrac{r_e E_3\mu}{2(1-\nu^2)}(\cos\alpha_0)^2 \\ K_{tc} = \dfrac{\tau_1[\cos\varphi\tan(\varphi+\beta-r_0)-\sin\varphi]}{\frac{\tau_1}{\tau_2}\cos(\theta-\varphi)\sin\theta-\sin(\theta-\varphi)\cos\theta} \\ K_{te} = \dfrac{\pi r_e E_3}{8(1-\nu^2)}(\cos\theta-\mu\sin\theta)+\dfrac{r_e E_3\mu}{2(1-\nu^2)}(1-\mu\cos\alpha_0\sin\alpha_0) \end{cases} \quad (13)$$

(2) Cutting force coefficients of plain-woven CFRP

In order to establish the cutting force model, the cutting chronological order of a single-layer woven fabric may be firstly investigated. The woven structure of a single-layer woven fabric and its cutting chronological order are presented in Fig. 4. The region of A' B′ D' C′ is a unit cell of a plain weave. It is dominated by the cutting of the fill fibers in the region of OAA'P and OBD'Q. This cutting model can be called as model I. On the other hand, the cutting of the warp fibers are dominated in the region of OBB'P and OAC'Q, which can be regarded as model II. If every layer of CFRP stacks so neatly and the alignments of

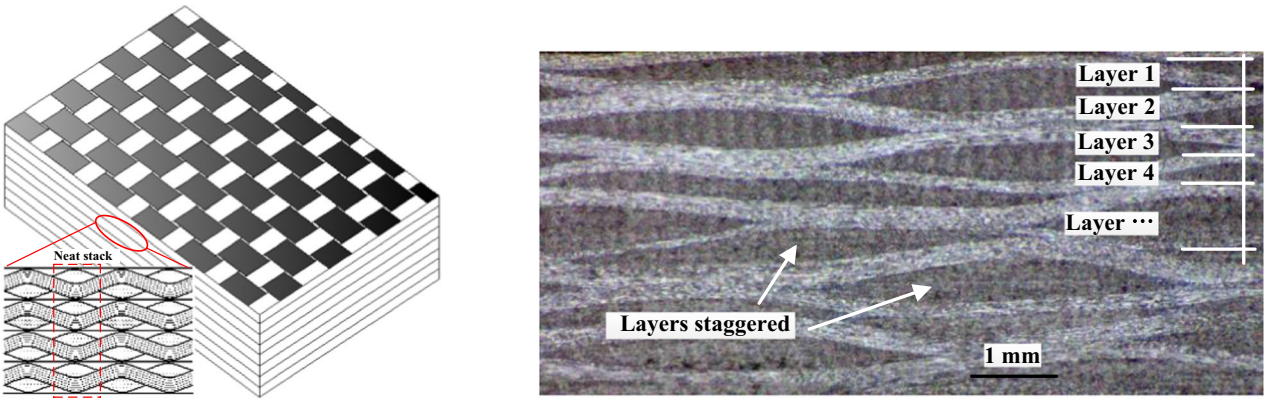

(a) Ideal structure of the plain-woven CFRP (b) Actual structure of the plain-woven CFRP

Fig. 5 Structure of the plain-woven CFRP. **a** Ideal structure of the plain-woven CFRP. **b** Actual structure of the plain-woven CFRP

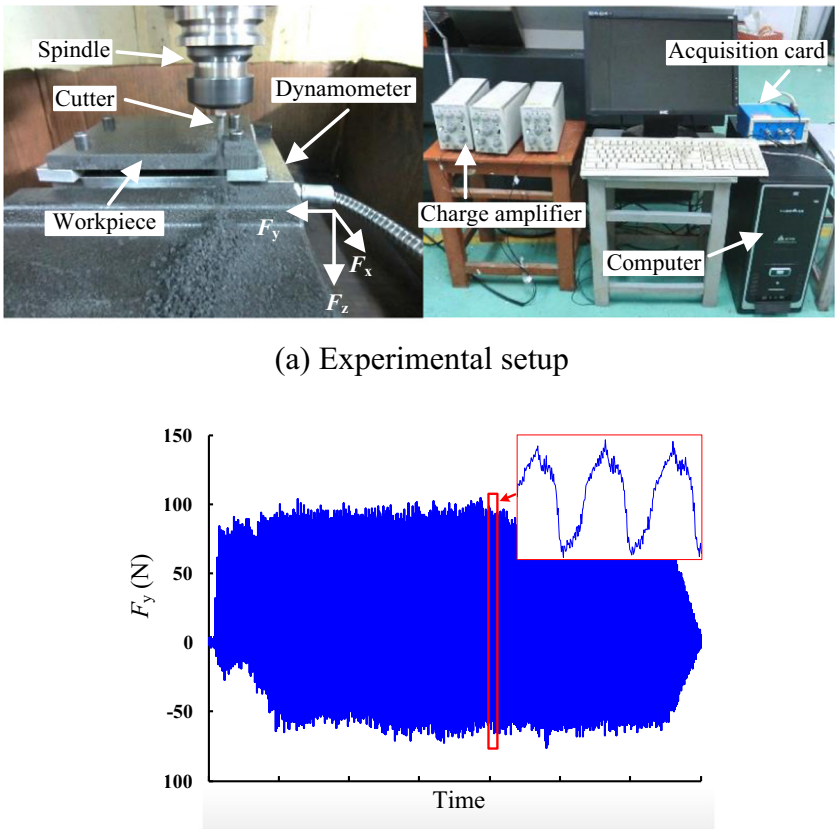

Fig. 6 Experimental setup and the typical forces. **a** Experimental setup. **b** Typical milling forces (F_y, V_c = 110 m/min, f_z = 0.1 mm/tooth, a_p = 1.2 mm)

the warp fibers and the fill fibers of each ply are good (as presented in Fig. 5a, the total cutting forces can be calculated with the cutting forces of each ply, according to this cutting chronological order of a single-layer woven fabric.

However, the warp fibers and the fill fibers of each ply are not stacked neatly, and there is a certain randomness during the stacking. As illustrated in Fig. 5b, the white long strip areas are the cross-sections of fill fibers and the black areas are the vertical sections of the warp fibers. As shown here, every layer of CFRP is mutually staggered, leading to irregular structure in the sections. Therefore, it is difficult to distinguish the cutting chronological order of each layer during the modeling. So, it is difficult to obtain the accurate cutting forces of each ply. But noteworthy, it can be found that the cutting model of a single-layer woven fabric tends to be half model I and half model II with different rotation angles, according to the above cutting model of a unit cell of a plain weave. So it suggests that the cutting force coefficients of the single layer can be treated as the coefficient means of model I and of model II, as given in Eq. (14). Then, substituting Eq. (14) into Eqs. (5) and (6), the X- and Y-direction milling forces can be solved.

$$\begin{cases} \overline{K_{rc}} = \dfrac{1}{2}\left[\dfrac{\tau_1[\sin\varphi\tan(\varphi+\beta-r_0)+\cos\varphi]}{\frac{\tau_1}{\tau_2}\cos(\theta_1-\varphi)\sin\theta_1-\sin(\theta_1-\varphi)\cos\theta_1}+\dfrac{\tau_1[\sin\varphi\tan(\varphi+\beta-r_0)+\cos\varphi]}{\frac{\tau_1}{\tau_2}\cos(\theta_2-\varphi)\sin\theta_2-\sin(\theta_2-\varphi)\cos\theta_2}\right] \\ \overline{K_{re}} = \dfrac{1}{2}\left[\dfrac{\pi r_e E_3}{8(1-\nu^2)}(\sin\theta_1+\mu\cos\theta_1)+\dfrac{\pi r_e E_3}{8(1-\nu^2)}(\sin\theta_2+\mu\cos\theta_2)\right]+\dfrac{r_e E_3\mu}{2(1-\nu^2)}(\cos\alpha_0)^2 \\ \overline{K_{tc}} = \dfrac{1}{2}\left[\dfrac{\tau_1[\cos\varphi\tan(\varphi+\beta-r_0)-\sin\varphi]}{\frac{\tau_1}{\tau_2}\cos(\theta_1-\varphi)\sin\theta_1-\sin(\theta_1-\varphi)\cos\theta_1}+\dfrac{\tau_1[\cos\varphi\tan(\varphi+\beta-r_0)-\sin\varphi]}{\frac{\tau_1}{\tau_2}\cos(\theta_2-\varphi)\sin\theta_2-\sin(\theta_2-\varphi)\cos\theta_2}\right] \\ \overline{K_{te}} = \dfrac{\pi r_e E_3}{16(1-\nu^2)}[(\cos\theta_1-\mu\sin\theta_1)+(\cos\theta_2-\mu\sin\theta_2)]+\dfrac{r_e E_3\mu}{2(1-\nu^2)}(1-\mu\cos\alpha_0\sin\alpha_0) \end{cases} \quad (14)$$

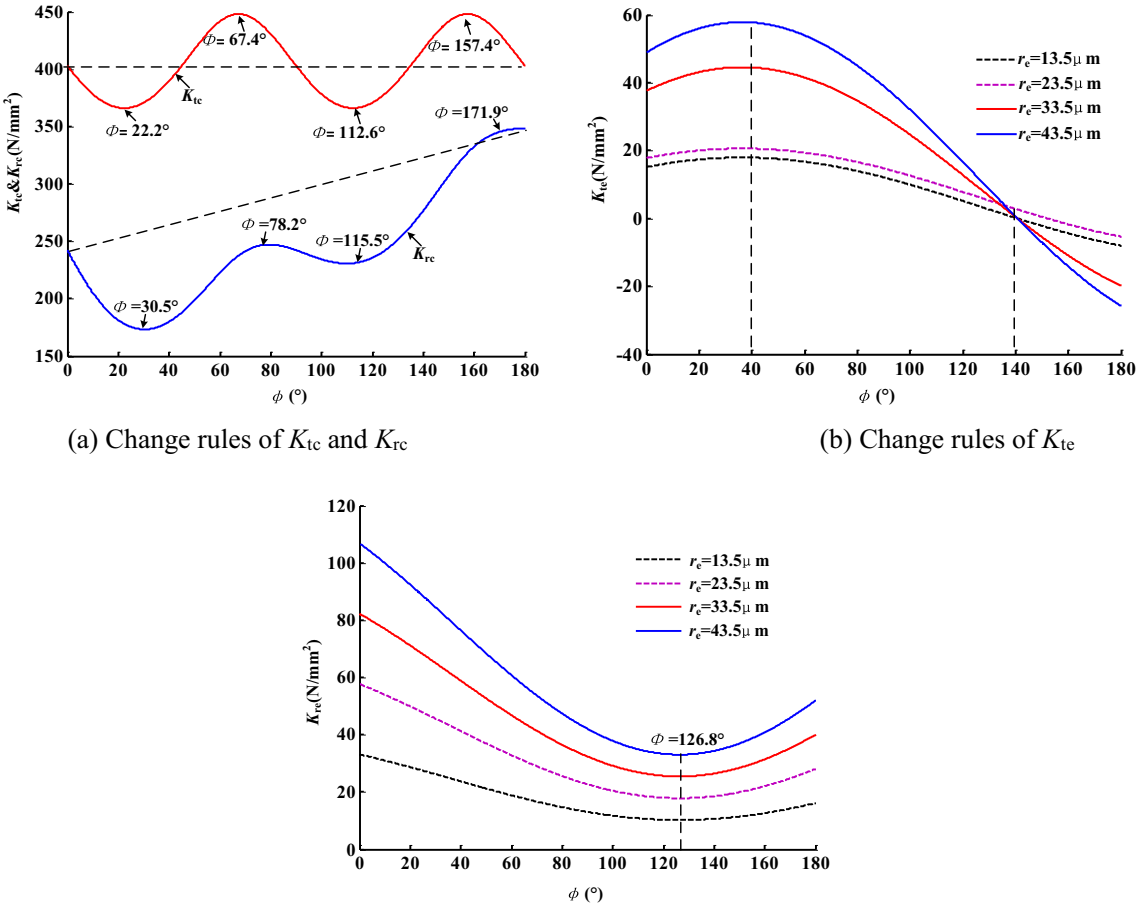

(a) Change rules of K_{tc} and K_{rc}

(b) Change rules of K_{te}

(c) Change rules of the K_{re}

Fig. 7 Relationship among φ, K_{tc}, K_{rc}, K_{te}, and K_{re}. **a** Change rules of K_{tc} and K_{rc}. **b** Change rules of K_{te}. **c** Change rules of the K_{re}

where $\overline{K_{tc}}$ and $\overline{K_{rc}}$ are the average cutting force coefficients in tangential and radial directions, respectivelyand $\overline{K_{te}}$ and $\overline{K_{re}}$ are the average corresponding edge force coefficients.

3 Experimental verification

Experimental studies were carried out on a KVC1050M NC vertical machining center without coolant. A brazed polycrystalline diamond (PCD) end mill with two flutes, zero helix, and the diameter of 6 mm was employed in these slotting experiments. A piezoelectric dynamometer (YDX-III9702) with supporting a multichannel charge amplifier (YE5850) was applied to measure the horizontal and vertical directions milling forces. The forces signals were stored and processed on a PC subsequently. The experimental setup and the force measurement systems were illustrated in Fig. 6a. A typical milling force in the Y-direction was shown in Fig. 6b.

A unidirectional carbon plain weave fabric/epoxy resin (T300/Epoxy) composite plate was applied during the experiments. The average thickness per layer was 0.2 mm and the total thickness was 10 mm. The width of a bundle of fiber was 2.5 mm. The fiber volume content was 60 ± 5%; the average diameter of carbon fibers was 7~8 μm. The milling length of each test was about 15~20 mm, so the effect on the material properties of the temperature was ignored. All the correlative material parameters were obtained at room temperature. The test samples had a modulus $E_3 = 3.45$ Gpa, a minor Poisson's ratio $\nu = 0.3$, the shear strength of the fiber $\tau_1 = 140$ MPa, and that of the matrix $\tau_2 = 75$ MPa. In the experiments, the fiction angle $\beta = 30°$, and the fiction coefficient $\mu = 0.15$, the normal rake angle $\gamma_0 = 0°$, clearance angle $\alpha_0 = 15°$, and the fillet radius of the principle cutting lip $r_e = 13.5$ μm.

4 Results and discussion

4.1 Cutting force coefficients for different rotation angles

The variations of the average cutting force coefficients (i.e., $\overline{K_{tc}}$ and $\overline{K_{rc}}$) and the average edge force coefficients (i.e., $\overline{K_{te}}$ and $\overline{K_{re}}$) with the rotation angle φ (0–180°) are presented in Fig. 7.

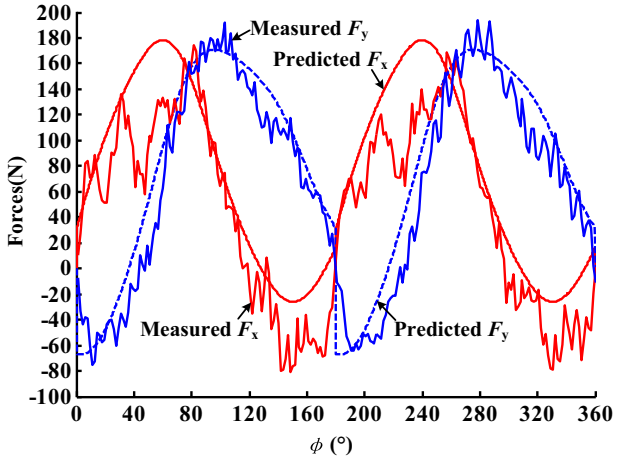

(a) Predicted milling forces in V_c=109m/min,f_z=0.18mm/tooth,a_p=2mm

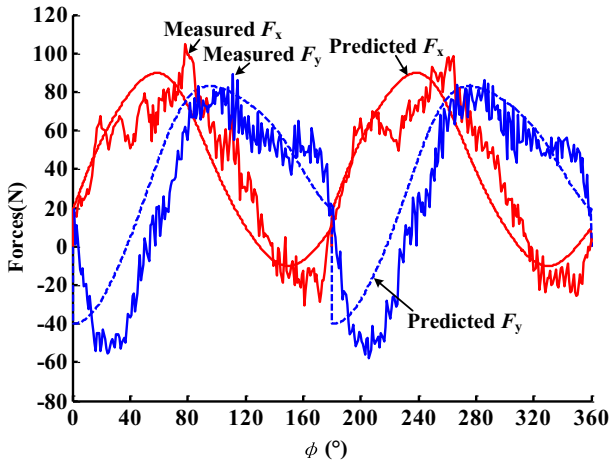

(b) Predicted milling forces in V_c=65m/min,f_z=0.14mm/tooth,a_p=1.2mm

Fig. 8 Simulated curves of milling force. **a** Predicted milling forces in V_c = 109 m/min, f_z = 0.18 mm/tooth, and a_p = 2 mm. **b** Predicted milling forces in V_c = 65 m/min, f_z = 0.14 mm/tooth, and a_p = 1.2 mm

As shown in Fig. 7a, the cutting force coefficients (i.e., $\overline{K_{tc}}$ and $\overline{K_{rc}}$) demonstrate cyclical fluctuation with the rotation angle. The rotation angles of the peak values of them are close to each other. Both of the cutting force coefficients (i.e., $\overline{K_{tc}}$ and $\overline{K_{rc}}$) have two low peaks when the rotation angle φ ranges from 20 to 30° and from 110 to 115°, as well as two high peaks when the rotation angle φ ranges from 67 to 78° and from 157 to 172°. Furthermore, the radial cutting force coefficients ($\overline{K_{rc}}$) increase gradually overall; nevertheless, the tangential cutting force coefficients ($\overline{K_{tc}}$) wobbles around a certain value. It can be proved again that the plain-woven CFRP has obvious anisotropic. Hence, as $90° \le \varphi \le 180°$, the milling forces increase gradually because of the effect of the radial cutting force coefficients ($\overline{K_{rc}}$).

When the rotation angle is less than 40°, as shown in Fig. 7a, c, the tangential edge force coefficients ($\overline{K_{te}}$) rises gradually with the increase of the rotation angle φ. In turn, it decreases gradually

Table 1 Comparison of predicted forces with experimental values in different feed per tooth

No.	a_c (mm)	f_z (mm/tooth)	F_x (N)			F_y (N)		
			Exp.	Pre.	% Deviation	Exp.	Pre.	% Deviation
1	1.2	0.02	49.4	41.3	16.4	29.8	24.3	18.4
2	1.2	0.06	61.2	56.4	7.9	47.5	43.9	7.6
3	1.2	0.1	80.0	72.9	8.9	65.5	63.4	3.2
4	1.2	0.14	92.1	89.8	2.5	80.9	82.9	2.5
5	1.2	0.18	111.1	107.0	3.7	98.2	102.5	4.4

Average absolute deviations of F_x (%) 7.9, and average absolute deviations of F_y (%) 7.2

Table 2 Comparison of predicted forces with experimental values in different cutting depths

No.	f_z (mm/tooth)	a_c (mm)	F_x (N)			F_y (N)		
			Exp.	Pre.	% Deviation	Exp.	Pre.	% Deviation
1	0.1	0.6	38.7	36.4	5.9	30.0	31.7	5.6
2	0.1	1.2	80.0	72.9	8.9	65.5	63.4	3.2
3	0.1	1.8	115.9	109.3	5.7	101.3	95.1	6.1
4	0.1	2.4	151.1	145.7	3.6	133.8	126.9	5.2
5	0.1	3	189.3	181.8	4.0	183.6	158.5	13.7

Average absolute deviations of F_x (%) 5.6, and average absolute deviations of F_y (%) 6.8

when the rotation angle is beyond 40°. On the other hand, the radial edge force coefficients ($\overline{K_{re}}$) decreases gradually when $0° \le \varphi \le 126°$; in contrast, it rises gradually when $126° < \varphi \le 180°$, but its increment is very small. Therefore, the influences of the edge force coefficients (i.e., $\overline{K_{re}}$ and $\overline{K_{te}}$) on the cutting forces decrease gradually during the cutting process of the single teeth. Generally speaking, both of the edge force coefficients rise with the increase of the cutter edge radius. It can be inferred that the cutting edge radius is lesser to result in the weaker effects of the edge force coefficients.

Over all, all the force coefficients (i.e., $\overline{K_{tc}}$, $\overline{K_{rc}}$, $\overline{K_{te}}$, and $\overline{K_{re}}$) regularly change with the rotation angle as a consequence of anisotropy of plain-woven CFRP. Besides, the average cutting force coefficients (i.e., $\overline{K_{tc}}$ and $\overline{K_{rc}}$) are the crucial factors affecting the cutting forces; by contrast, the average edge force coefficients (i.e., $\overline{K_{re}}$ and $\overline{K_{te}}$) have a poor effect on the cutting forces, but have a greater influence with the increment of tool wear.

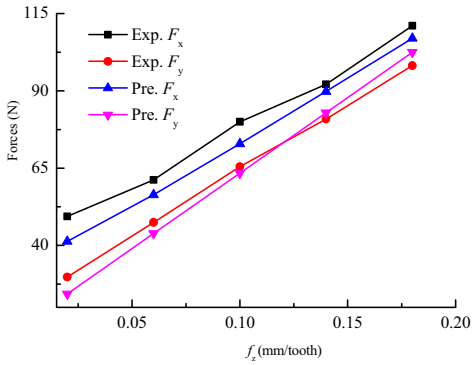

(a) Relationship between the forces and the feed per tooth

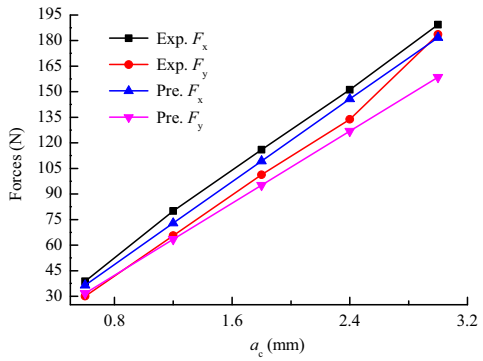

(b) Relationship between the forces and the cutting depth

Fig. 9 Relationship among the forces, the feed per tooth, and the cutting depth. **a** Relationship between the forces and the feed per tooth. **b** Relationship between the forces and the cutting depth

4.2 Validation of the milling force model

As a view to validate the theoretical model derived above, the theoretical predictions are compared with the cutting forces measured at variable cutting velocity (V_c = 63~110 m/min), variable feed rate (f_z = 0.02~0.18 mm/tooth), and variable cutting depth (a_p = 0.6~3 mm).

As shown in Fig. 8a, b, it can be seen that the model predictions and the experimental measurements agree well with each other except the partial difference. Variance between the predicted and experimental result is due to following reasons:

- It is only considered the fiber fracture mode when the fiber orientation $\theta \le 90°$, but instead of that as the fiber orientation $\theta > 90°$, during orthogonal cutting modeling for the individual segments.
- There may be errors in the extracted time points between the measured and the simulated results.
- To some extent, there are some differences between the experimental cutting depth and the theoretical one, owing to the cutting vibration.

In total, both the change tendencies of the experimental and theoretical curves are in qualitative agreement with each other. Beyond that, the max-mean values of the measured curves and the maximum values of the simulation curves (positive) are nearly equal to each other, as listed in Tables 1 and 2. As illustrated in Fig. 9a, b, both of the cutting forces F_x and F_y increase with increasing the cutting depth a_p or the feed rate f_z; this change tendencies of the predictions are basically corresponding to that of the measured values. It is shown that all the average absolute values of relative errors between predictive and measured cutting force values are less than 10%. Obviously, the changing rule reflected by the theoretical results coincides well with the

measuring data. And the maximal average of the cutting forces can be successfully predicted. This theoretical model has good prediction ability about the cutting forces.

But additionally, when the model is simplified, the influence of the cutting speed V_c on the cutting forces may be ignored in this theoretical model. As a result, the cutting forces at the same cutting depth or feed rate may be basically the same as each other, although the cutting speed is different. Usually, the cutting speed is a key factor effecting on the friction coefficient, the tool wear, the cutting temperature, etc. [34]. Thus, these affect complexly the cutting forces. In this paper, the effects of the friction coefficient, the tool wear, the cutting temperature, etc., on the cutting forces are appropriately ignored, owing to the good abrasion resistance of the PCD end mill and the short milling length of each test. Analytical results discussed by Li [34] indicate the functional relation between the cutting speed V_c and the friction coefficient μ, as given in Eq. (15). In theory, the change rules of the cutting forces with the cutting speed can be obtained by substituting Eq. (15) into Eq. (14). But this functional relation may be subject to change due to the different cutting conditions of the actual manufacturing. Therefore, the accurate simulation curves may only be obtained when this functional relationship is clearly identified, according to the actual conditions of the milling. Additionally, comparing with the cutting depth a_p and the feed rate f_z, the effect of the cutting speed V_c has less influence on the cutting forces. Based on the abovementioned reasons, in this paper, the influence of the cutting speed V_c on the cutting forces has been ignored in this theoretical model to simplify the modeling. In the future research, the functional relation between the cutting speed V_c and the friction coefficient μ under different cutting conditions is accurately acquired as one of the important researches. Furthermore, the effect of cutting speed on the cutting forces also deserves to be studied more deeply in the future:

$$\mu = 3.633\overline{\sigma}^{-0.484} V_c^{-0.119} \tag{15}$$

where $\overline{\sigma}$ is the average contact stress.

5 Conclusions

The following conclusions can be drawn from the work presented in this paper:

1. All the force coefficients (i.e., $\overline{K_{tc}}$, $\overline{K_{rc}}$, $\overline{K_{te}}$, and $\overline{K_{re}}$) regularly change with the rotation angle during the cutting of plain-woven CFRP. The average cutting force coefficients (i.e., $\overline{K_{tc}}$ and $\overline{K_{rc}}$) are the crucial factors affecting the cutting forces; by contrast, the average edge force coefficients (i.e., $\overline{K_{re}}$ and $\overline{K_{te}}$) have a poor effect on the cutting forces, but have a greater influence with the increment of tool wear.
2. The changing rule reflected by the theoretical results well agrees with the measuring data, and the maximal average of the cutting forces can be successfully predicted. All the average absolute values of relative errors between predictive and measured values of the max-means of the cutting forces are less than 10%. Therefore, this theoretical model has good prediction ability about the cutting forces.

Acknowledgements Special thanks to the National Science Foundation of China (No. 51675285) for funding this work.

References

1. Jia Z, Fu R, Niu B, Qian B, Bai Y, Wang F (2016) Novel drill structure for damage reduction in drilling CFRP composites [J]. Int J Mach Tool Manu 110:55–65. https://doi.org/10.1016/j.ijmachtools.2016.08.006
2. Bonnet C, Poulachon G, Rech J, Girard Y, Costes JP (2015) CFRP drilling: fundamental study of local feed force and consequences on hole exit damage [J]. Int J Mach Tool Manu 94:57–64. https://doi.org/10.1016/j.ijmachtools.2015.04.006
3. Gaugel S, Sripathy P, Haeger A, Meinhard D, Bernthaler T, Lissek F, Kaufeld M, Knoblauch V, Schneider G (2016) A comparative study on tool wear and laminate damage in drilling of carbon-fiber reinforced polymers (CFRP) [J]. Compos Struct 155:173–183. https://doi.org/10.1016/j.compstruct.2016.08.004
4. Wang F, Qian B, Jia Z et al (2017) Secondary cutting edge wear of one-shot drill bit in drilling CFRP and its impact on hole quality [J]. Compos Struct 178:341–352
5. Zitoune R, Mansori ME, Krishnaraj V (2013) Tribo-functional design of double cone drill implications in tool wear during drilling of copper mesh/CFRP/woven ply [J]. Wear 302(1–2):1560–1567. https://doi.org/10.1016/j.wear.2013.01.046
6. Liu J, Chen G, Ji C, Qin X, Li H, Ren C (2014) An investigation of workpiece temperature variation of helical milling for carbon fiber reinforced plastics (CFRP) [J]. Int J Mach Tool Manu 86(11):89–103. https://doi.org/10.1016/j.ijmachtools.2014.06.008
7. Wang CY, Chen YH, An QL, Cai XJ, Ming WW, Chen M (2015) Drilling temperature and hole quality in drilling of CFRP/aluminum stacks using diamond coated drill [J]. Int J Precis Eng Manuf 16(8):1689–1697. https://doi.org/10.1007/s12541-015-0222-y
8. Kalla D, Sheikh-Ahmad J, Twomey J (2010) Prediction of cutting forces in helical end milling fiber reinforced polymers [J]. Int J Mach Tools Manuf 50(10):882–891
9. Karimi NZ, Heidary H, Minak G (2016) Critical thrust and feed prediction models in drilling of composite laminates [J]. Compos Struct 148:19–26. https://doi.org/10.1016/j.compstruct.2016.03.059
10. Slamani M, Chatelain JF, Hamedanianpour H (2015) Comparison of two models for predicting tool wear and cutting force components during high speed trimming of CFRP [J]. Int J Mater Form 8(2):305–316. https://doi.org/10.1007/s12289-014-1170-2
11. Fernandes M, Cook C (2006) Drilling of carbon composites using a one shot drill bit. Part I: five stage representation of drilling and factors affecting maximum force and torque [J]. Int J Mach Tool Manu 46(1):70–75. https://doi.org/10.1016/j.ijmachtools.2005.03.015
12. Wang M, Gao L, Zheng Y (2014) An examination of the fundamental mechanics of cutting force coefficients [J]. Int J Mach Tool Manu 78(1):1–7. https://doi.org/10.1016/j.ijmachtools.2013.10.008

13. Rubeo MA, Schmitz TL (2016) Mechanistic force model coefficients: a comparison of linear regression and nonlinear optimization [J]. Precis Eng 45:311–321. https://doi.org/10.1016/j.precisioneng.2016.03.008
14. Li Zhongqun(2008) Dynamic modeling, simulation and optimization of high speed milling under complicated cutting conditions. [D] Beijing: Beihang University
15. Sheikh-Ahmad J, Twomey J, Kalla D et al (2007) Multiple regression and committee neural network force prediction models in milling FRP [J]. Mach Sci Technol 11(3):391–412
16. Karpat Y, Bahtiyar O, Değer B (2012) Mechanistic force modeling for milling of undirectional carbon fiber reinforced polymer laminates [J]. Int J Mach Tools Manuf 56:79–93. https://doi.org/10.1016/j.ijmachtools.2012.01.001
17. Shengchao H, Yan C, Xu J et al (2014) Modeling and simulation of milling forces in side milling multi-layer CFRP with multitooth cutter [J]. Acta Materiae Compositae Sinica 31(5):1375–1381
18. Luo Z, Zhao W, Li J et al (2016) Cutting force modeling in end milling of curved geometries based on oblique cutting process [J]. J Mech Eng 52(9):184–192. https://doi.org/10.3901/JME.2016.09.184
19. Takeyama H, Iijima N (1988) Machinability of glass fiber reinforced plastics and application of ultrasonic machining [J]. CIRP Ann Manuf Technol 37(1):93–96. https://doi.org/10.1016/S0007-8506(07)61593-5
20. Bhatnagar N, Ramakrishnan N, Naik NK, Komanduri R (1995) On the machining of fiber reinforced plastic (FRP) composite laminates [J]. Int J Mach Tool Manu 35(5):701–716. https://doi.org/10.1016/0890-6955(95)93039-9
21. Zhang LC, Zhang HJ, Wang XM (2001) A force prediction model for cutting unidirectional fibre-reinforced plastics. Mach Sci Technol 5(3):293–305. https://doi.org/10.1081/MST-100108616
22. Jahromi AS, Bahr B (2010) An analytical method for predicting cutting forces in orthogonal machining of unidirectional composites [J]. Compos Sci Technol 70(16):2290–2297. https://doi.org/10.1016/j.compscitech.2010.09.005
23. Qi Z, Zhang K, Cheng H, Wang D, Meng Q (2015) Microscopic mechanism based force prediction in orthogonal cutting of unidirectional CFRP [J]. Int J Adv Manuf Technol 79(5–8):1209–1219. https://doi.org/10.1007/s00170-015-6895-7
24. Chen L, Zhang K, Cheng H, et al (2017) A cutting force predicting model in orthogonal machining of unidirectional CFRP for entire range of fiber orientation [J]. Int J Adv Manuf Technol 89:833–846
25. Xu W, Zhang LC (2014) On the mechanics and material removal mechanisms of vibration-assisted cutting of unidirectional fibre-reinforced polymer composites [J]. Int J Mach Tools Manuf 80–81(5):1–10
26. Xu W, Zhang L (2016) Mechanics of fibre deformation and fracture in vibration-assisted cutting of unidirectional fibre-reinforced polymer composites [J]. Int J Mach Tool Manu 103:40–52. https://doi.org/10.1016/j.ijmachtools.2016.01.002
27. Niu B, Su Y, Yang R, Jia Z (2016) Micro-macro-mechanical model and material removal mechanism of machining carbon fiber reinforced polymer [J]. Int J Mach Tool Manu 111:43–54. https://doi.org/10.1016/j.ijmachtools.2016.09.005
28. Guo DM, Wen Q, Gao H et al (2011) Prediction of the cutting forces generated in the drilling of carbon-fibre-reinforced plastic composites using a twist drill [J]. Proc Inst Mech Eng B J Eng Manuf 226(1):28–42
29. Sánchez NF, Díaz-Álvarez A, Cantero JL et al (2015) Experimental analysis of special tool geometries when drilling woven and multidirectional CFRPs [J]. J Reinf Plast Compos 19(19):1215–1220
30. Parsian A, Magnevall M, Beno T, Eynian M (2014) A mechanistic approach to model cutting forces in drilling with indexable inserts [J]. Procedia Cirp 24:74–79. https://doi.org/10.1016/j.procir.2014.07.138
31. Wang H, Qin XA (2016) Mechanistic model for cutting force in helical milling of carbon fiber-reinforced polymers [J]. Int J Adv Manuf Technol 82(9–12):1485–1494
32. Karpat Y, Bahtiyar O, Değer B (2012) Milling force modelling of multidirectional carbon fiber reinforced polymer laminates [J]. Procedia Cirp 1(1):460–465. https://doi.org/10.1016/j.procir.2012.04.082
33. Fu Z, Yang W, Wang X, Leopold J (2015) Analytical modelling of milling forces for helical end milling based on a predictive machining theory [J]. Procedia Cirp 31:258–263. https://doi.org/10.1016/j.procir.2015.03.013
34. Li GY (2011) Research on defects generation mechanism and process optimization in drilling laminated composite [D]. Jinan: Shandong University